Intermittent dynamics in externally driven ferroelastics and strain glasses

Marcel Porta,[1] Teresa Castán,[2] Pol Lloveras,[3] Avadh Saxena,[4] and Antoni Planes[2]

[1]*Departament de Física Quàntica i Astrofísica, Facultat de Física, Universitat de Barcelona. Martí i Franquès 1, 08028 Barcelona, Catalonia*

[2]*Departament de Física de la Matèria Condensada, Facultat de Física, Universitat de Barcelona. Martí i Franquès 1, 08028 Barcelona, Catalonia*

[3]*Departament de Física, EEBE, Campus Diagonal-Besòs and Barcelona Research Center in Multiscale Science and Engineering, Universitat Politècnica de Catalunya. Eduard Maristany 10-14, 08019 Barcelona, Catalonia*

[4]*Theoretical Division, Los Alamos National Laboratory, Los Alamos, New Mexico 87545, USA*

(Received 4 May 2018; published 28 September 2018)

The interplay of elastic anisotropy and disorder dictates many of the properties of ferroic materials, specifically martensites. We use a phase-field model for ferroelastic athermal materials to study their response to an increasing external stress that couples to the strain order parameter. We show that these systems evolve through avalanches and study the avalanche-size distribution for ferroelastic systems (large anisotropy and/or small disorder) and for the strain glass (small anisotropy and/or large disorder) using various statistical analysis techniques, including the maximum likelihood method. The model predicts that in the former case the distribution is subcritical or power law (in agreement with experimental observations), whereas in the latter case it becomes supercritical. Our results are consistent with experiments on martensitic materials, and we predict specific avalanche behavior that can be tested and used as an alternative means to characterize strain glasses.

DOI: 10.1103/PhysRevE.98.032143

I. INTRODUCTION

Disorder is a key factor for the occurrence of inherent inhomogeneities in ferroic materials on a mesoscopic spatial scale [1]. Usually these textures precede a phase transition to the ferroic phase and are thus signatures of the incoming ground state [2]. Relaxor ferroelectrics [3] and random magnets [4] are well-known examples of materials displaying this behavior. In ferroelastic materials these kinds of precursors are also known from a very long time. They usually show up in the form of cross-hatched modulation patterns, denoted as tweed [5], which are embedded in the high temperature phase matrix. Therefore, precursor states are multiphase states, which consist of coexisting regions with properties varying over nanometer distances.

In this class of ferroic materials, the presence of disorder gives rise to a distribution of energy barriers that, in some circumstances, is responsible for the suppression of the transition to the long-range ordered ferroic state due to the breakdown of the correlation effects [6–9]. Then, the inhomogeneous state becomes frozen and the system displays glassy features. This behavior is well known to occur in the case of relaxor ferroelectrics and magnetic cluster glasses. More recently it has been shown to occur in some ferroelastic-martensitic systems as well [10], where it takes place mainly due to kinetic arrest rather than geometrical frustration [11–13]. In these materials it has been reported that above a certain critical amount of disorder, which has been shown to depend on the strength of an anisotropic long-range elastic interaction [13], the transition to the twinned ferroelastic structure is suppressed and glassy behavior ensues giving rise to a strain-glass phase [6,14–16]. Glassy behavior occurs because while local transformations to the ferroic phase take place at short timescales, coalescence into a global phase requires much longer times, which tend to diverge as temperature is lowered [12]. Consequently, more and more time is required for the system to reach for paths leading to the final state. This is indeed the mechanism giving rise to kinetic arrest in this class of materials.

It is known that within the glassy phase, application of an external field that couples to the order parameter (magnetic, polar, structural) enables us to induce the otherwise inhibited long-range ordered phase. The existence of disorder together with the minor role played by thermal fluctuations suggests that these externally driven systems should display an intermittent, stochastic dynamics (or crackling noise) [17]. This means that the system may respond to changes of the external driving conditions through discrete, impulsive events spanning a broad range of sizes. Therefore, it is expected that strain glasses evolve through a sequence of transition events that can be described as an *avalanche* process. In fact, such an intermittent avalanche dynamics has been reported to occur associated with martensitic transitions induced both thermally and by application of an external field (stress) in many different materials [18,19].

It has been confirmed that often the avalanches occur with the absence of characteristic scales. Actually, this scale-free intermittent dynamics is then known as avalanche criticality. An interesting result is that for this class of out-of-equilibrium criticality to occur, some models suggest that a critical amount of disorder is required [17], which has been experimentally corroborated in a few cases [20]. This fact immediately suggests the following question: Is this amount of disorder related to the amount needed for glassy behavior to occur? This is the main issue that we address in the present paper. To this end, a phase-field model for a ferroelastic

transition is used [2,13,14]. The model includes disorder and an anisotropic long-range interaction and follows a purely relaxational athermal dynamics. It was previously found that the amount of disorder required for glassy behavior to occur scales with the square root of the elastic anisotropy, which controls the strength of the long-range elastic interaction [13]. In the present work we study the response of the model system to an increasing external stress in both the martensite and the strain-glass phase. At low temperature criticality is found in the boundary separating both phases as well as in the martensite phase. In contrast, in the strain-glass phase the distribution of avalanches is supercritical [21]. At higher temperatures, as the transition from these phases to the high symmetry phase (austenite) is approached, the distribution of avalanches in the martensite phase is consistent with a subcritical distribution whereas in the strain-glass phase the distribution remains supercritical.

The paper is organized as follows. The strain based martensitic model is summarized in Sec. II. Section III presents the numerical simulation results dealing with the dynamics of the system driven by an applied external stress. The statistical analysis of the avalanches obtained in the stress driven evolution is given in Sec. IV. Finally, Sec. V provides a general discussion of the results and concludes.

II. MODEL

The model used was introduced previously with the purpose of studying various textures (or microstructure) in ferroelastics [2,13,14]. In this section we summarize its main features.

The starting point is a strain-based two-dimensional (2D) Ginzburg-Landau free-energy density for the square-to-rectangle structural transition that includes local coupling to quenched disorder. We recall that for this transformation the three available elastic modes are $e_1 = (\varepsilon_{xx} + \varepsilon_{yy})/\sqrt{2}$ (bulk dilatation), $e_2 = (\varepsilon_{xx} - \varepsilon_{yy})/\sqrt{2}$ (deviatoric strain), and $e_3 = \varepsilon_{xy}$ (shear strain), where ε_{ij} are the components of the linear strain tensor. First, we write an expansion of the free-energy density in terms of the deviatoric strain only, which is the order parameter of the transition,

$$f_{\mathrm{GL}} = \tfrac{1}{2}A_2(T)e_2^2 - \tfrac{1}{4}\beta e_2^4 + \tfrac{1}{6}\gamma e_2^6 + \tfrac{1}{2}\kappa|\vec{\nabla}e_2|^2 - \sigma_2 e_2, \quad (1)$$

where the deviatoric stress, defined as $\sigma_2 = (\sigma_{xx} - \sigma_{yy})/\sqrt{2}$, is the externally applied field. The harmonic coefficient A_2 is related to the elastic constant $C' = (C_{11} - C_{12})/2 = A_2/2$ and it is assumed to vary linearly with temperature, $A_2 = a(T - T_c)$, with $a > 0$ and T_c being the lower stability limit of the square phase. The coefficients β and γ are higher-order elastic constants and together with the parameter κ are taken to be positive. The disorder is introduced via the harmonic coefficient, A_2, in a manner that is equivalent to introducing a spatial dependence of the stability limit of the square phase, $T_c(\mathbf{r})$, and therefore of the transition temperature, $T_0(\mathbf{r})$. That is,

$$T_c(\mathbf{r}) = \overline{T_c}[1 + \eta(\mathbf{r})], \quad (2)$$

where $\eta(\mathbf{r})$ is a Gaussian distributed random variable with zero mean, standard deviation ζ, and spatially correlated with an exponential pair correlation function with correlation length ξ,

$$\langle \eta(\mathbf{r})\eta(\mathbf{r}')\rangle = \zeta^2 \exp(-|\mathbf{r} - \mathbf{r}'|/\xi). \quad (3)$$

The spatial variation of the stability limit is intended to reproduce the statistical fluctuations of composition in materials. In addition, the spatial correlation of the disorder ensures that such variations are smooth.

Another important ingredient is the effective long-range strain interaction. Its origin lies in the contribution from the non-order-parameter strain components arising from the coherent matching between nearby transformed unit cells. Consequently, we add to Eq. (1) the simplest expansion in e_1 and e_3,

$$f = f_{\mathrm{GL}} + \tfrac{1}{2}A_1 e_1^2 + \tfrac{1}{2}A_3 e_3^2, \quad (4)$$

where the coefficients $A_1 = C_{11} + C_{12}$ and $A_3 = 4C_{44}$ are again second-order elastic constants. Notice that the local free-energy density $f(\mathbf{r})$ is a functional of the strain fields $e_1(\mathbf{r})$, $e_2(\mathbf{r})$, and $e_3(\mathbf{r})$. These are linked by the Saint-Venant's compatibility condition, which ensures the integrity of the lattice [22]. Minimization of the integral free energy,

$$F = \int d\mathbf{r} f(\mathbf{r}), \quad (5)$$

with respect to the non-order-parameter strain components, $e_1(\mathbf{r})$ and $e_3(\mathbf{r})$, with the constraint of compatibility yields the free-energy density as a function of the order parameter only. That is,

$$f(\mathbf{r}) = f_{\mathrm{GL}}(\mathbf{r}) + \frac{1}{2}\int e_2(\mathbf{r})U(\mathbf{r} - \mathbf{r}')e_2(\mathbf{r}')d\mathbf{r}'. \quad (6)$$

Interestingly, $U(\mathbf{r} - \mathbf{r}')$ is a long-range kernel that, in Fourier space, is given by

$$\hat{U}(\mathbf{k}) = A_3 \frac{\left(k_x^2 - k_y^2\right)^2}{\left(\frac{A_3}{A_1}\right)\left(k_x^2 + k_y^2\right)^2 + 8k_x^2k_y^2}. \quad (7)$$

This expression embodies the anisotropic character of the free energy and is minimized when the strain modulations are oriented along $\langle 11\rangle$ directions ($k_x = \pm k_y$). The magnitude of such a long-range anisotropic term is directly proportional to the elastic coefficient A_3, provided that the ratio A_3/A_1 is constant. Notice that the elastic anisotropy factor is $\mathcal{A} = C_{44}/C' = A_3/2A_2$, so that at constant temperature $\mathcal{A} \sim A_3$. This energy term enhances the correlation of the order parameter at different locations. On the contrary, the disorder (characterized by ζ) inhibits such correlations. Once the model is discretized, the interplay between the disorder and the long-range interaction yields a distribution of energy barriers that the system has to cope with to minimize its energy. Depending on the structure of such a distribution of energy barriers the low temperature phase is either martensitic or a strain glass. Thus, by varying the model parameter A_3 and in conjunction with the disorder the model predicts a crossover from a twinned martensite to a strain-glass phase [13,14]. This is illustrated in Fig. 1 where we plot the boundary separating both phases in the A_3-ζ parameter space.

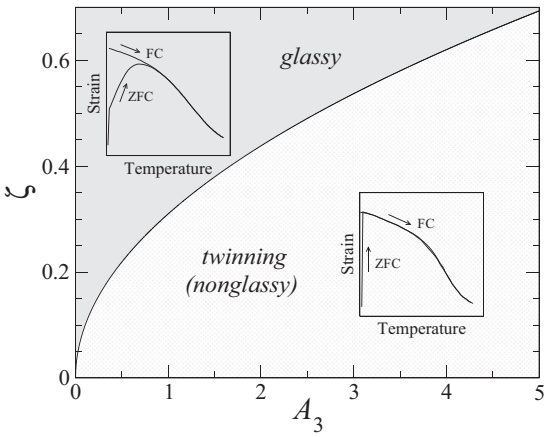

FIG. 1. Phase diagram of the model presented in Sec. II in the A_3-ζ parameter space. The strain-glass phase is stabilized for large values of disorder (ζ) or small values of elastic anisotropy ($\mathcal{A} \sim A_3$). The insets show examples of the ZFC/FC strain curves that were used to distinguish the strain-glass phase from the martensite phase.

Such boundary was determined in Ref. [13] from the behavior of the zero-field-cooled and field-cooled (ZFC/FC) strain curves.

A large deviation between these curves at low temperature is commonly associated with glassy behavior [23]. Representative examples are shown in the insets of Fig. 1. These correspond to the simulation of a small system where the size of the elastic domains is of the order of the size of the simulation cell, especially in the martensite phase. Thus, as soon as a stress is applied before heating, a jump in the strain is obtained in the ZFC curves. We also note that the first-order martensite-austenite transition becomes smooth because of the distribution of transition temperatures (disorder). The strain-glass phase corresponds to those values of the disorder and elastic anisotropy that yield a large splitting of the ZFC/FC curves.

Avalanche behavior is usually related to athermal and rate independent dynamics to a good approximation [24]. For this class of dynamics, thermal fluctuations are irrelevant compared to the high energy barriers separating metastable states. Thus, in order that the dynamics can proceed it is necessary to drive the system externally with a field that couples to the order parameter (stress, in our case). Keeping this in mind, we define the fluctuationless relaxational dynamics,

$$\frac{\partial e_2(\mathbf{r})}{\partial t} = -\Gamma \frac{\delta F}{\delta e_2(\mathbf{r})}, \tag{8}$$

where the relationship between the strain components due to compatibility is taken into account in the functional derivative of the free energy with respect to the deviatoric strain, which yields anisotropic and nonlocal elastic forces [see Eq. (6)].

All physical quantities are given in the reduced units defined in Ref. [2].

The size of the simulation cell is $L \times L = 1000 \times 1000$ except otherwise stated, and the discretization parameter is $\Lambda = 1.9531$, so that the simulation cell is discretized onto a 512×512 mesh. The elastic anisotropy, controlled by the parameter A_3, is varied in our simulations while the ratio A_3/A_1 and the strength of the disorder are fixed to $A_3/A_1 = 2$ and $\zeta = 0.22$. The remaining model parameters are the same as in Ref. [2].

III. THERMOMECHANICAL TREATMENT AND INTERMITTENT RESPONSE

In this section we describe the thermomechanical protocol applied to the model and study its intermittent response through avalanches.

First of all, we generate a disordered configuration with a small amount of strain which is consistent with the high temperature, high symmetry phase (austenite).

This configuration is thermally quenched to $T = 0.2T_c$ and fully relaxed [25] in the absence of external stresses using the relaxational dynamics defined in Eq. (8).

Then, an increasing deviatoric stress is applied at constant temperature.

We start with a stress $\sigma_2 = 10^{-8}$ and the strain field is fully relaxed to the new equilibrium configuration, which ensures that the dynamics is rate independent (adiabatic limit).

This last step is repeated iteratively; the applied stress is increased by an amount $\delta\sigma_2 = 10^{-8}$ and the strain configuration is relaxed. This yields a stress-strain relation where the average strain eventually responds to the applied stress through jumps.

That is, infinitesimal increments of the applied stress may produce finite changes in the average strain. This is what we denote as avalanches. This behavior is shown in Fig. 2 where we plot a stress-strain curve corresponding to $A_3 = 0.1$.

Notice in the inset, where a small portion of the stress-strain relation is enlarged, that periods of elastic response (shown as thick continuous lines) are separated by jumps in the average strain (indicated by dashed lines).

This is qualitatively similar to the stress-strain relation obtained at larger scales. This self-similarity suggests the

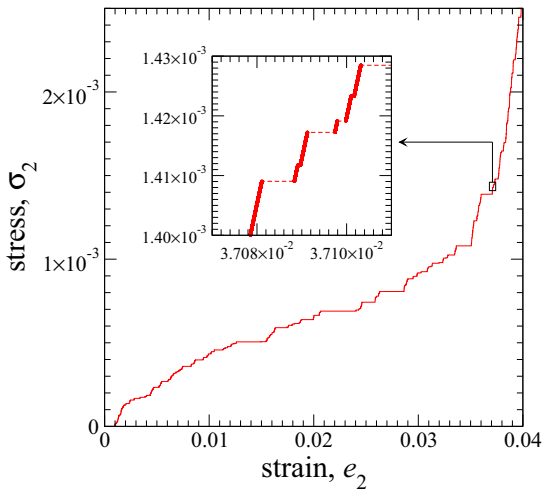

FIG. 2. Stress-strain relation of a strain glass ($A_3 = 0.1$, $\zeta = 0.22$) obtained by thermal quench of a disordered strain configuration to $T = 0.2T_c$. The inset shows an enlarged fraction of the curve where jumps (avalanches) of the equilibrium strain induced by small increments of the applied stress are clearly visible.

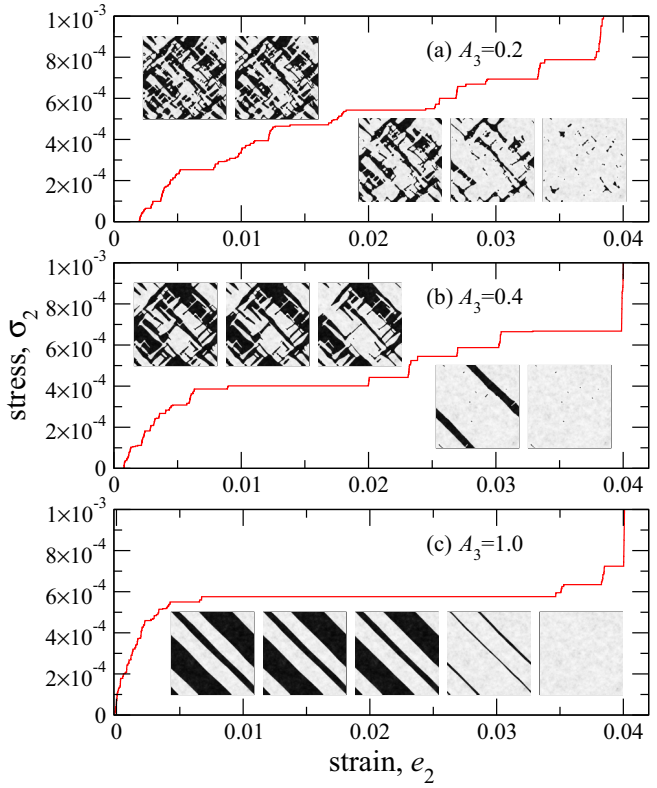

FIG. 3. Stress-strain relation in the strain-glass phase (a), in the ferroelastic (martensite) phase (c), and at the crossover between these phases (b) in the A_3-ζ parameter space. In all cases the initial microstructure is generated by the thermal quench of a disordered strain configuration to $T = 0.2T_c$. Snapshots of the strain configuration for $\sigma_2 = 0$, $\sigma_2 = 2 \times 10^{-4}$, $\sigma_2 = 4 \times 10^{-4}$, $\sigma_2 = 6 \times 10^{-4}$, and $\sigma_2 = 8 \times 10^{-4}$ (from left to right) are also shown.

absence of a characteristic length (or avalanche size) in a given strain range.

According to the phase diagram shown in Fig. 1, depending on the model parameter A_3 the obtained strain configurations correspond to a martensite phase (low-symmetry low-temperature phase) or a strain glass. Thus, the stress-strain curves qualitatively depend on this parameter. In Fig. 3 we show a typical stress-strain curve in the strain-glass phase [$A_3 = 0.2$, Fig. 3(a)], in the martensite phase [$A_3 = 1.0$, Fig. 3(c)], and near the boundary between both phases [$A_3 = 0.4$, Fig. 3(b)].

We find that for quenches into the martensite phase the system responds with large avalanches at a characteristic yield stress, whereas for the other values of the applied stress the avalanche sizes are smaller. This establishes several stress regimes, namely low-stress, yield-stress, and high-stress regimes.

In contrast, when the system is quenched into the strain-glass phase, the distribution of avalanche sizes is less correlated with the magnitude of the applied stress. As the crossover from the martensite phase to the strain-glass phase is smooth, the correlation between the applied stress and the size of the avalanches also decreases smoothly from the martensite phase to the strain glass phase. For illustrational purposes in Fig. 3 we also depict several snapshots of the

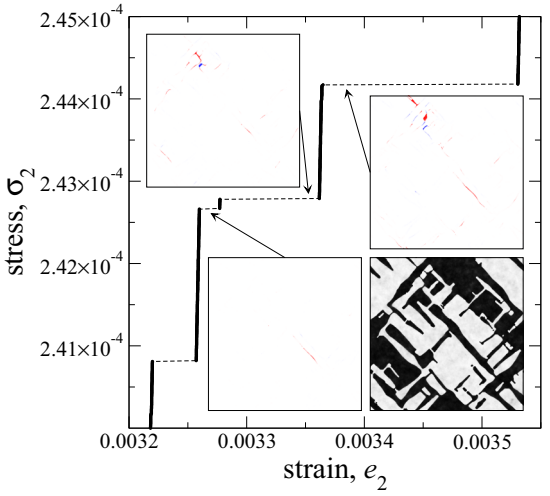

FIG. 4. Snapshots of the strain field change that occurs in single avalanches for $A_3 = 0.4$ in the low stress regime. Arrows indicate the corresponding jump in the stress-strain curve. Red indicates positive strain variation, white indicates no strain variation, and blue stands for negative strain variation. As a reference, in the right bottom corner we show the strain configuration before the avalanches, shown in the snapshots, occur.

strain configuration corresponding to the applied stresses (from left to right) $\sigma_2 = 0$, $\sigma_2 = 2 \times 10^{-4}$, $\sigma_2 = 4 \times 10^{-4}$, $\sigma_2 = 6 \times 10^{-4}$, and $\sigma_2 = 8 \times 10^{-4}$.

In Figs. 4 and 5 we show snapshots of the deviatoric strain variation that occurs in single avalanches for $A_3 = 0.4$. This is computed as the difference between the strain field before and after a given avalanche has occurred.

The corresponding stress-strain curve is also shown with arrows indicating the jump in the average strain associated with each one of the snapshots. We use a color scale, where red indicates positive strain variation, white indicates no strain variation, and blue stands for negative strain variation. As a

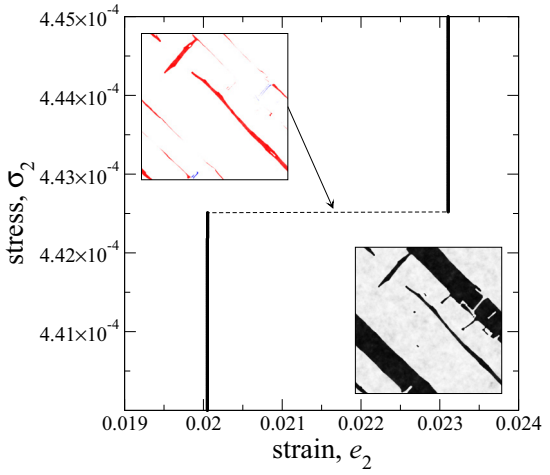

FIG. 5. Snapshot of the strain field change that occurs in a single avalanche for $A_3 = 0.4$ in the yield stress regime. The color scale is the same as in Fig. 4. As a reference, in the right bottom corner we show the strain configuration before the avalanche, shown in the snapshot, occurs.

reference, in the right bottom corner of each figure we show the strain configuration before the avalanches, shown in the snapshots, occur. Figure 4 shows avalanches corresponding to the small stress regime. We obtain that small avalanches are associated with local changes in the strain configuration, mainly to the displacement of a single twin boundary. Larger avalanches, on the contrary, are associated with global changes of the strain field; many twin boundaries in different locations move simultaneously generating a single strain jump. This cooperative behavior is more evident in Fig. 5 where we depict a single, and much larger, avalanche in the yield stress regime. In this case we observe the displacement of twin boundaries occurring simultaneously with the flipping of entire domains.

IV. STATISTICAL ANALYSIS OF THE AVALANCHES

In this section we analyze the statistical properties of the avalanches. This study requires a large number of events. Thus, for each set of model parameters the thermomechanical protocol described above is repeated $n = 64$ times. For each one of the runs we use a different configuration of the quenched disorder and start from a different initial strain configuration. This procedure ensures that a large number of avalanches is available without having to deal with large systems.

A first insight into the probability distribution of the avalanche sizes is obtained graphically by plotting the number of avalanches obtained versus the associated strain variation using logarithmically binned data. This is shown in Fig. 6 for different values of the elastic anisotropy, controlled by the parameter A_3.

The results are consistent with a power-law probability distribution in a limited strain variation regime, $\Delta e_{2\min} < \Delta e_2 < \Delta e_{2\max}$,

$$P[\Delta e_2 < X < \Delta e_2 + d(\Delta e_2)] \propto {\Delta e_2}^{-\alpha} d(\Delta e_2). \quad (9)$$

The exponent of the power-law distribution, α, can be determined by a least-squares fit, shown in Fig. 6 as a red line. We note that because of the logarithmic binning of the data the slope of the distribution of avalanches in the log-log plot is one unit smaller than the exponent α.

For $\Delta e_2 < \Delta e_{2\min}$ the number of avalanches decays when decreasing the strain variation.

This occurs because there is a minimum size for the avalanches, which depends on characteristic lengths of the model such as the width of the domain boundaries or the correlation length of the disorder. As the strain is computed as an intensive quantity the larger the size of the simulation cell the smaller the strain variation that can be detected. Thus, $\Delta e_{2\min}$ depends on the size of the simulation cell, L, as well. To avoid any ambiguity we denote as avalanche size the scaled strain variation, $L^2 \Delta e_2$. With this definition the minimum avalanche size of the power-law regime, $L^2 \Delta e_{2\min}$ is independent of the size of the simulation cell, as we will show below.

The largest strain variation that can occur is a jump from a single variant with strain $-e_2^{\rm eq}$ to a single variant with strain $+e_2^{\rm eq}$, where $e_2^{\rm eq}$ is the equilibrium strain at the corresponding temperature. If the effect of the applied stress is neglected, the equilibrium strain can be approximated as

$$e_2^{\rm eq} \approx \sqrt{\frac{\beta + \sqrt{\beta^2 - 4\gamma A_2}}{2\gamma}}. \quad (10)$$

Thus,

$$\Delta e_{2\max} \approx 2\sqrt{\frac{\beta + \sqrt{\beta^2 - 4\gamma A_2}}{2\gamma}}. \quad (11)$$

Using this approximation, the current values of the model parameters yield $\Delta e_{2\max} \approx 0.08$. Thus, the largest strain variations observed, which are of the order of $\Delta e_2 \sim 10^{-2}$, correspond to the flip of large domains and are only observed once or twice for each run.

For quenches into the martensite phase we obtain that $\Delta e_{2\max} \sim e_2^{\rm eq}$, and the distribution of avalanches ends around this value. However, for quenches into the strain-glass phase $\Delta e_{2\max}$ is substantially smaller, and the deviation from the power-law distribution expands over a large range of avalanche sizes (see the distribution for $A_3 = 0.1$). This raises the question of whether the avalanches may have a non-power-law distribution in the strain-glass phase or rather this deviation is due to finite size effects.

To clarify this point, for $A_3 = 0.1$ we have plotted the distribution of avalanche sizes for three different sizes of

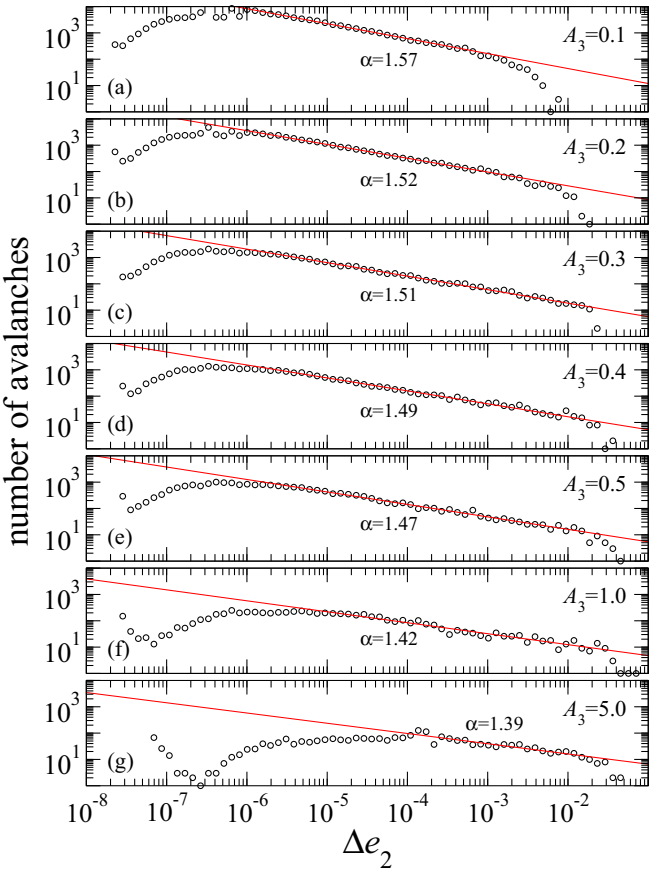

FIG. 6. Log-log plot of the number of avalanches versus the strain variation for $A_3 = 0.1$ (a), $A_3 = 0.2$ (b), $A_3 = 0.3$ (c), $A_3 = 0.4$ (d), $A_3 = 0.5$ (e), $A_3 = 1.0$ (f), and $A_3 = 5.0$ (g). The red line in each plot is a least-squares fit to a power-law relation.

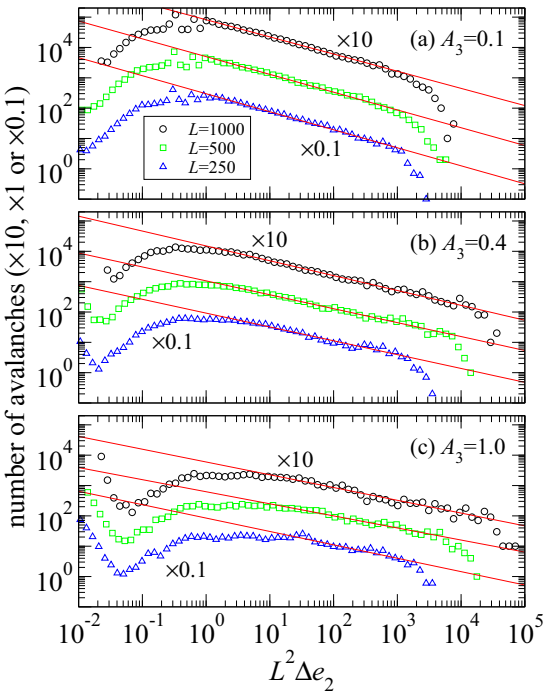

FIG. 7. Number of stress induced avalanches versus the avalanche size for three different sizes of the simulation cell ($L = 1000$, $L = 500$ and $L = 250$) and three different values of the elastic constant A_3 [$A_3 = 0.1$ (a), $A_3 = 0.4$ (b), and $A_3 = 1.0$ (c)] using the same discretization parameter, $\Lambda = 1.9531$, in all cases. The red lines are least-square fits to a power-law relation. The number of independent simulations performed is $n = 64$, $n = 128$, and $n = 256$ for $L = 1000$, $L = 500$, and $L = 250$, respectively.

the simulation cell, using the same discretization parameter in all cases. For completeness this study is also performed for $A_3 = 1.0$ and $A_3 = 0.4$, which correspond to quenches into the martensite phase and the boundary between this phase and the strain-glass phase, respectively. The results are shown in Fig. 7 where we denote the avalanche size as the scaled strain variation as defined above. As expected, we find that $L^2\Delta e_{2\min}$ and the distribution of avalanches for $\Delta e_2 < \Delta e_{2\min}$ is independent of the size of the simulation cell for all values of A_3 considered, as the distribution of small avalanches should not depend on the size of the system.

On the contrary, in general, $L^2\Delta e_{2\max}$ depends on the size of the simulation cell. For quenches into the martensite phase and the boundary between this phase and the strain-glass phase ($A_3 = 1$ and $A_3 = 0.4$, respectively) $L^2\Delta e_{2\max}$ scales to a good approximation as

$$L^2\Delta e_{2\max} \sim L^2. \tag{12}$$

Thus, the distribution of avalanche sizes is consistent with a power law with an upper cutoff determined by the size of the simulation cell. On the contrary, for quenches into the strain-glass phase ($A_3 = 0.1$) $L^2\Delta e_{2\max}$ is almost independent of the size of the simulation cell, and thus the drop of the number of avalanches for $\Delta e_2 > \Delta e_{2\max}$ cannot be related to the size of the system. Therefore, the distribution of avalanches is supercritical. In this case, the value of $\Delta e_{2\max}$ must depend on other characteristic lengths of the system such as the size of the domains that are stabilized by the energy barriers that arise from the disorder.

The distribution of avalanche sizes has also been analyzed using a maximum likelihood method [26]. We consider the likelihood function,

$$\mathcal{L}(\alpha) = \prod_{i=1}^{N} p(\Delta e_{2i}, \alpha), \tag{13}$$

where the normalized probability density $p(\Delta e_2, \alpha)$ with $\Delta e_{2\min} < \Delta e_2 < \Delta e_{2\max}$ is assumed to be power law,

$$p(\Delta e_2, \alpha) = \frac{1-\alpha}{\Delta e_{2\max}^{1-\alpha} - \Delta e_{2\min}^{1-\alpha}} \Delta e_2^{-\alpha}. \tag{14}$$

The exponent α is obtained as the value that maximizes the logarithm of the likelihood function, $\ln \mathcal{L}(\alpha)$, which is the solution of the equation,

$$\sum_{i=1}^{N} \ln \Delta e_{2i} + \frac{N}{1-\alpha} - \frac{N}{\Delta e_{2\max}^{1-\alpha} - \Delta e_{2\min}^{1-\alpha}} \times \left(\Delta e_{2\max}^{1-\alpha} \ln \Delta e_{2\max} - \Delta e_{2\min}^{1-\alpha} \ln \Delta e_{2\min}\right) = 0, \tag{15}$$

where N is the total number of avalanches obtained in the n runs with $\Delta e_{2\min} < \Delta e_2 < \Delta e_{2\max}$ and Δe_{2i} is the variation of the deviatoric strain obtained in the ith avalanche.

In Figs. 8(a)–8(g) we plot the exponent of the power-law distribution obtained with the likelihood method as a function of $\Delta e_{2\max}$ for a fixed value of $\Delta e_{2\min}$, as indicated in the figure. A clear plateau is obtained for $0.2 \leqslant A_3 \leqslant 0.5$ with an exponent $\alpha = 1.50 \pm 0.05$. For $A_3 \geqslant 1$ the number of avalanches obtained is small, and consequently the uncertainty is too large to conclude unambiguously if a plateau exists.

For $A_3 = 0.1$ the effective exponent depends on the upper cutoff and, as concluded above, the distribution is not consistent with a power law.

In Figs. 8(h)–8(n) we plot the exponent of the power-law distribution obtained with the likelihood method as a function of $\Delta e_{2\min}$. In this case, the upper cutoff, $\Delta e_{2\max}$, is fixed to the value obtained from Figs. 8(a)–8(g) and from the log-log plots of the avalanche size distribution shown in Fig. 6.

Again, a plateau is obtained only for $0.2 \leqslant A_3 \leqslant 0.5$. For $A_3 \geqslant 1$ the number of avalanches obtained is not sufficient to draw conclusions.

For $\zeta = 0.22$, which is the amount of disorder used in the present work, the splitting between the field-cooled and the zero-field-cooled curves that was used to distinguish the strain-glass phase from the martensite phase [13] typically occurs at temperatures $T < 0.5T_c$, depending on the value of A_3. Thus, it is insightful to see if above the splitting temperature the distribution of avalanches in the strain-glass phase is also different from the distribution in the martensite phase.

To this end, we study the distribution of stress induced avalanches when the thermal quench is performed to $T = 0.8T_c$, near the ferroelastic phase transition. The number of avalanches obtained versus the associated strain variation is plotted in Fig. 9 for several values of the elastic anisotropy using logarithmically binned data.

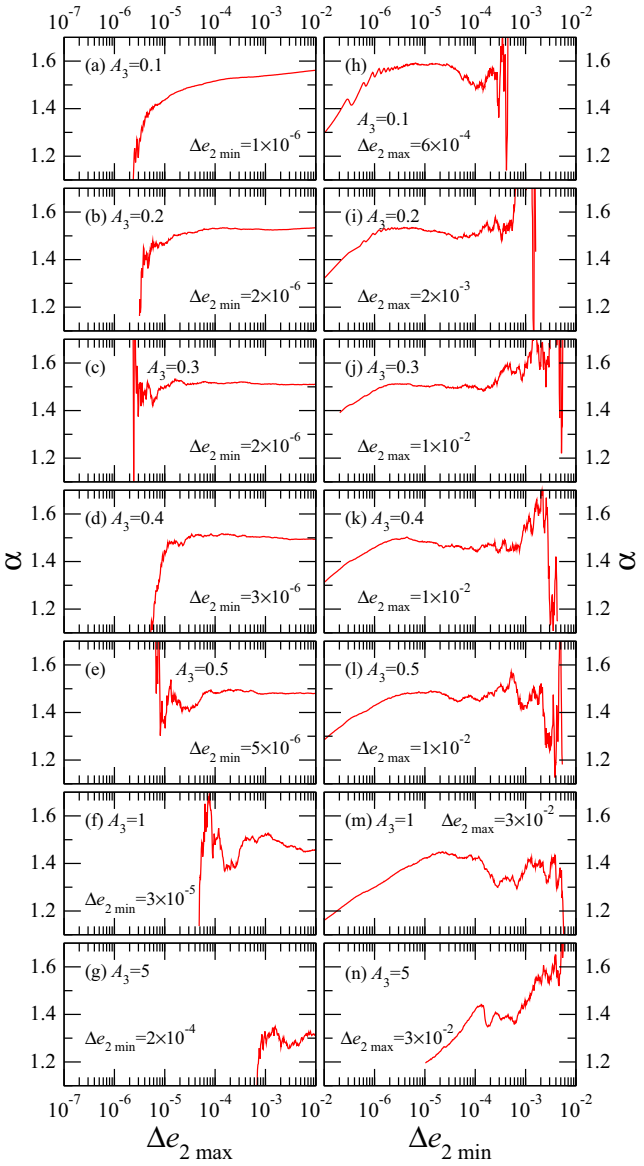

FIG. 8. (a–g) Exponent α of the power-law probability distribution $P \sim \Delta e_2{}^{-\alpha}$ versus $\Delta e_{2\max}$ for a fixed value of $\Delta e_{2\min}$. (h–n) Exponent α of the power-law probability distribution $P \sim \Delta e_2{}^{-\alpha}$ versus $\Delta e_{2\min}$ for a fixed value of $\Delta e_{2\max}$.

For quenches into the strain-glass phase the result is qualitatively similar to the results obtained at the lower temperature $T = 0.2T_c$. On the contrary, for quenches into the martensite phase ($A_3 \gtrsim 0.3$), at $T = 0.8T_c$ we obtain an excess amount of large avalanches superimposed to the power-law distribution that was not obtained at $T = 0.2T_c$. This excess of large avalanches can be characterized as a peak in the distribution of avalanche sizes. We have also studied how these results depend on the size of the simulation cell.

In Fig. 10 we show the distribution of avalanche sizes for quenches into the strain-glass phase [$A_3 = 0.1$, Fig. 10(a)] and the martensite phase [$A_3 = 1.0$, Fig. 10(b)] for $L = 1000$, $L = 500$, and $L = 250$, using the same discretization parameter in all cases. For quenches into the strain-glass phase we find that the upper cutoff of the power-law distribution is

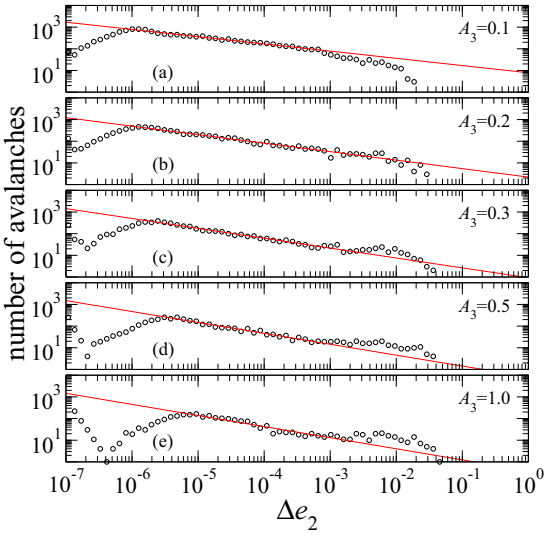

FIG. 9. Log-log plot of the number of avalanches versus the strain variation obtained after a thermal quench to $T = 0.8T_c$. The red line in each plot is a least-squares fit to a power-law relation.

almost independent of the size of the simulation cell. Therefore, as obtained at the lower temperature $T = 0.2T_c$, the distribution of avalanche sizes is supercritical. For quenches into the martensite phase we analyze the dependence of the position of the peak in the distribution of avalanche sizes on

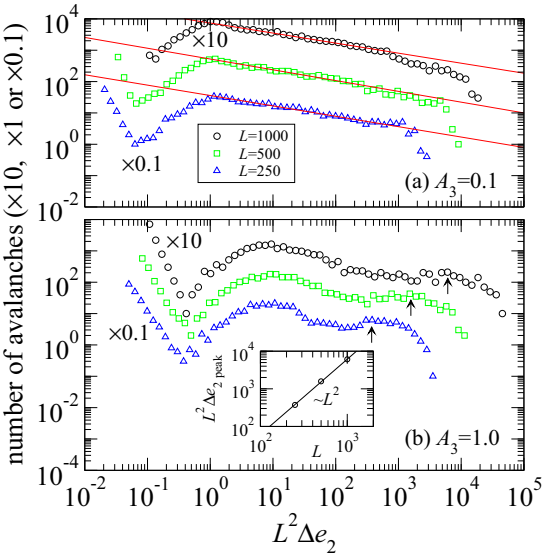

FIG. 10. Number of stress induced avalanches versus the avalanche size after a quench to $T = 0.8T_c$ for three different sizes of the simulation cell ($L = 1000$, $L = 500$, and $L = 250$) and two values of the elastic constant A_3 [$A_3 = 0.1$ (a) and $A_3 = 1.0$ (b)] using the same discretization parameter, $\Lambda = 1.9531$, in all cases. The red lines are least-square fits to a power-law relation. The number of independent simulations performed is $n = 64$, $n = 128$, and $n = 256$ for $L = 1000$, $L = 500$, and $L = 250$, respectively. The inset shows the scaling relation between the position of the peak in the distribution of avalanche sizes for $A_3 = 1.0$ and the size of the simulation cell.

the size of the simulation cell. This position, indicated with arrows in the figure, scales approximately as

$$L^2 \Delta e_{2\text{peak}} \sim L^2. \tag{16}$$

This is consistent with a subcritical distribution of avalanche sizes as it indicates that a few avalanches have a characteristic size that is proportional to the size of the simulation cell. Thus, we conclude that at $T = 0.8T_c$ criticality is only obtained at the crossover between the martensite and the strain-glass phases.

V. DISCUSSION AND CONCLUSIONS

In this work, we have sought to establish a realistic framework based on a phase-field model suitable to describe low-temperature avalanche dynamics in stress-driven martensitic and ferroelastic systems.

Although the model is formulated in 2D it corresponds to a projection of the three-dimensional (3D) models suitable for the cubic-to-tetragonal or tetragonal-to-orthorhombic transitions [22]. It takes into account the effects of long-range anisotropic interactions arising from elastic compatibility constraints, and quenched disorder, which is assumed to originate from composition fluctuations. In the model, the microstructure of the low-temperature phase reached by cooling from high temperature is controlled by the ratio of the amount of disorder, measured by the standard deviation of its distribution, and the strength of the long-range interaction, which is proportional to the elastic anisotropy of the system. In particular, fixing the amount of disorder, for low anisotropy the system gets frozen in a strain-glass phase, while for high anisotropy a twinned martensitic phase forms. We have numerically investigated the athermal strain response of these systems when driven by an externally applied stress. We have found that due to the existence of disorder the system evolves toward a single variant martensite through strain jumps, which define avalanches.

In all cases, avalanches distribute in a broad range of sizes. However, a detailed study demonstrates that the distribution is supercritical when starting from a deep strain-glass phase and becomes critical, and thus characterized by a power-law distribution, only when starting from close enough to the boundary that separates glassy from twinned martensitic behavior in the phase diagram. In fact, criticality occurs in a broad crossover region that seems to have an excursion rather inside the interior of the twinned martensitic region. In any case, results suggest that for large enough anisotropy or very low amount of disorder, subcritical behavior must occur. Indeed, this is consistent with the analytical solution of the clean limit.

The main idea behind supercritical and subcritical dynamics is the following. Subcritical dynamics would correspond to a situation with a low density of energy barriers where the long-range interaction, which induces long-range strain correlations, dominates over the disorder. In this case, the transformation of a small domain induces the transformation of neighboring domains and this effect propagates to relatively long distances giving rise to very large avalanches characterized by a certain length scale related to the scale of the system. Supercritical dynamics, in contrast, corresponds to a situation with a high density of energy barriers where the disorder dominates over the long-range interaction. Thus, the disorder is expected to be able to break the correlations and suppress the possibility of propagation of local transformations. The dynamics in this case is controlled by small avalanches with a characteristic length scale.

In general, avalanche dynamics is accepted to be inherent to any externally driven, athermal disordered system [17]. Beyond martensitic transitions, avalanches have been reported to occur during magnetization processes [27,28], plastic deformation [29], or failure under compression of inhomogeneous materials [30,31], among many others. Usually, simple lattice models such as the random field Ising model (RFIM) [32] or the random bond Ising model (RBIM) [33] with athermal local relaxation dynamics (which is in fact equivalent to the dynamics used in the present study) are employed to simulate the field-driven behavior of these systems. Compared with such models, our model has the advantage of properly taking into account symmetry properties of both parent and martensitic phases, and thanks to incorporating long range effects due to which our model is able to reproduce the actual microstructure that grows at the transition. The main result obtained from lattice models is that criticality occurs for a given critical amount of disorder. Indeed, this result is also reproduced by the present model, which has been based on specific properties of the low-temperature phase.

It is worth reminding that in some cases, avalanches have also been studied using models less simplified than the simple lattice models mentioned above. An interesting approach based on a phase-field model was reported by Ahluwalia and Ananthakrishna in Ref. [34]. They also took into account the long-range effects to model a 2D system undergoing a martensitic transition. The aim of the paper was modeling acoustic emission (AE) avalanches that occur during thermally induced martensitic transitions. Actually, the AE is related to the strain avalanches, and the authors assumed that it can be taken into account from the dissipation associated with the movement of the parent-product interfaces, which was modeled by a Rayleigh dissipative functional. The authors were able to reproduce the power-law behavior of the statistical distribution of the amplitudes, energy, and duration of the AE avalanches. Compared to our work, the results reported in that paper would correspond to avalanches expected in the high anisotropy and low disorder limit.

To our knowledge, no experiments have been reported so far of avalanche behavior in stress-driven strain-glass phases. In systems transforming to twinned martensitic phases, experimental results based on AE measurements suggest that the distribution of AE avalanches tends to be power law in systems with a sufficiently large amount of disorder [20]. The power-law behavior reflects the absence of characteristic scales and thus corroborates the existence of avalanche criticality. AE experiments suggest that the exponents that identify the power law show weak universality, depending essentially on the symmetry change taking place at the transition. More specifically, they depend on the ratio R of symmetry operations of the high and low temperature phases [18]. So far, it is not yet clear to which extent the exponents depend on dimensionality. The presently studied 2D square-to-rectangle transition mimics a 3D cubic-to-tetragonal transition. For this

change of symmetry, an amplitude exponent, $\alpha_{3D} = 2.0 \pm 0.3$, has been determined experimentally [18,35]. The critical exponent obtained in our work is smaller than the 3D experimental exponent ($\alpha_{2D} \equiv \alpha = 1.50 \pm 0.05 \leqslant \alpha_{3D}$) as expected since the ratio R is 2 in our case instead of 3 in the real 3D case (two low temperature martensitic variants exist instead of three). However, small differences could also arise from the different dimensionality or from the symmetry breaking effects of the applied field that effectively reduces the ratio R. A detailed analysis is certainly needed to clarify this point further.

In summary, the results presented in this work confirm the relevance in martensitic and in general ferroelastic systems of the competition between long-range anisotropic elastic interaction and quenched disorder, which controls not only characteristic features of the domain pattern formed at the transition but also their dynamics under an applied stress field. We expect that the simulation results reported in the present paper provide guidance on how to proceed experimentally, to verify the ideas and predictions presented here, and in particular corroborate the crossover from supercritical to critical behavior at the boundary of strain-glass behavior. The study of avalanches could provide an interesting alternative method to characterize strain glasses.

ACKNOWLEDGMENTS

This research was supported by the Spanish Ministry of Science and FEDER under Projects No. MAT2016-75823-R and No. FIS2017-82625-P, by the Catalan Government under Project No. 2017SGR-42, and in part by the US Department of Energy. We thank E. Vives for useful comments.

[1] E. Dagotto, Complexity in strongly correlated electronic systems, Science **309**, 257 (2005).

[2] P. Lloveras, T. Castán, A. Planes, and A. Saxena, Precursor Nanoscale Textures in Ferroelastic Martensites, in *Disorder and Strain-Induced Complexity in Functional Materials*, edited by T. Kakeshita, T. Fukuda, A. Saxena, and A. Planes, Springer Series in Materials Science (Springer-Verlag, Heidelberg, 2012), Vol. 148, Chap. 12.

[3] S. Zhang and F. Li, High performance ferroelectric relaxor-$PbTiO_3$ single crystals: Status and perspective, J. Appl. Phys. **111**, 031301 (2012).

[4] S. Bedanta and W. Kleemann, Supermagnetism, J. Phys. D: Appl. Phys. **42**, 013001 (2009).

[5] D. Schryvers and L. E. Tanner, On the interpretation of high-resolution electron-microscopy images of premartensitic microstuctures in the Ni-Al β_2 phase, Ultramicroscopy **32**, 241 (1990).

[6] X. Ren, Y. Wang, K. Otsuka, P. Lloveras, T. Castán, M. Porta, A. Planes, and A. Saxena, Ferroelastic nanostructures and nanoscale transitions: Ferroics with point defects, MRS Bull. **34**, 838 (2009).

[7] Y. Nii, T. Arima, H. Y. Kim, and S. Miyazaki, Effect of randomness on ferroelastic transitions: Disorder-induced hysteresis loop rounding in Ti-Nb-O martensitic alloy, Phys. Rev. B **82**, 214104 (2010).

[8] Y. Ni, Z. Zhang, D. Wang, Y. Wang, and X. Ren, The effect of point defects on ferroelastic phase transition of lanthanum-doped calcium titanate ceramics, J. Alloys Compd. **577**, S468 (2013).

[9] B. Ramachandran, P. C. Chang, Y. K. Kuo, C. Chien, and S. K. Wu, Characteristics of martensitic and strain-glass transitions of the Fe-substituted TiNi shape memory alloys probed by transport and thermal measurements, Sci. Rep. **7**, 16336 (2017).

[10] S. Sarkar, X. Ren, and K. Otsuka, Evidence for Strain Glass in the Ferroelastic-Martensitic System $Ti_{50-x}Ni_{50+x}$, Phys. Rev. Lett. **95**, 205702 (2005).

[11] P. Lloveras, T. Castán, M. Porta, A. Saxena, and A. Planes, *Mesoscopic Modelling of Strain Glass*, edited by T. Lookman and X. Ren, in *Frustrated Materials and Ferroic Glasses* (Springer, Heidelberg, 2018).

[12] A. Planes, P. Lloveras, T. Castán, A. Saxena, and M. Porta, Ginzburg-Landau modelling of precursor nanoscale textures in ferroelastic materials, Continuum Mech. Thermodyn. **24**, 619 (2012).

[13] P. Lloveras, T. Castán, M. Porta, A. Planes, and A. Saxena, Glassy behavior in martensites: Interplay between elastic anisotropy and disorder in zero-field-cooling/field-cooling simulation experiments, Phys. Rev. B **80**, 054107 (2009).

[14] P. Lloveras, T. Castán, M. Porta, A. Planes, and A. Saxena, Influence of Elastic Anisotropy on Structural Nanoscale Textures, Phys. Rev. Lett. **100**, 165707 (2008).

[15] X. Ren, Y. Wang, Y. M. Zhou, Z. Zhang, D. Wang, G. L. Fan, K. Otsuka, T. Suzuki, Y. C. Ji, J. Zhang, Y. Tian, S. Hou, and X. D. Ding, Strain glass in ferroelastic systems: Premartensitic tweed versus strain glass, Philos. Mag. **90**, 141 (2010).

[16] Y. Ji, D. Wang, Y. Wang, Y. Zhou, D. Xue, K. Otsuka, Y. Wang, and X. Ren, Ferroic glasses, npj Comput. Mater. **3**, 43 (2017); (and references therein).

[17] J. P. Sethna, K. A. Dahmen, and C. R. Myers, Crackling noise, Nature **410**, 242 (2001).

[18] A. Planes, L. Mañosa, and E. Vives, Acoustic emission in martensitic transformations, J. Alloys Compd. **577**, S699 (2013).

[19] E. K. H. Salje and K. A. Dahmen, Crackling noise in disordered materials, Annu. Rev. Condens. Matter Phys. **5**, 233 (2014).

[20] F. J. Pérez-Reche, M. Stipcich, E. Vives, L. Mañosa, A. Planes, and M. Morin, Kinetics of martensitic transitions in Cu-Al-Mn under thermal cycling: Analysis at multiple length scales, Phys. Rev. B **69**, 064101 (2004).

[21] A system departing slightly from criticality will be denoted as subcritical when characterized by one or more avalanches spanning a macroscopic fraction of the system, and supercritical when all the avalanches are small—limited by a characteristic cutoff size. Only at criticality no characteristic scale is expected.

[22] T. Lookman, S. R. Shenoy, K. Ø. Rasmussen, A. Saxena, and A. R. Bishop, Ferroelastic dynamics and strain compatibility, Phys. Rev. B **67**, 024114 (2003).

[23] Y. Wang, X. Ren, K. Otsuka, and A. Saxena, Evidence for broken ergodicity in strain glass, Phys. Rev. B **76**, 132201 (2007).

[24] F. J. Pérez-Reche, E. Vives, L. Mañosa, and A. Planes, Athermal Character of Structural Phase Transitions, Phys. Rev. Lett. **87**, 195701 (2001).

[25] The criterion used to decide if a strain configuration is fully relaxed is a condition on the strain change that occurs in a single iteration of the relaxational algorithm.

[26] H. Bauke, Parameter estimation for power-law distributions by maximum likelihood methods, Eur. Phys. J. B **58**, 167 (2007).

[27] P. J. Cote and L. V. Meisel, Self-Organized Criticality and the Barkhausen Effect, Phys. Rev. Lett. **67**, 1334 (1991).

[28] G. Durin and S. Zapperi, *The Barkhausen Effect*, edited by G. Bertotti and I. D. Mayergoyz, in *The Science of Hysteresis*, Vol. II, Chap. 3 (Academic Press, San Diego, 2006), pp. 181–267.

[29] F. F. Csikor, C. Motz, D. Weygand, M. Zaiser, and S. Zapperi, Dislocation avalanches, strain bursts, and the problem of plastic forming at the micrometer scale, Science **318**, 251 (2007).

[30] J. Baró, A. Corral, X. Illa, A. Planes. E. K. H. Salje, W. Schranz, D. E. Soto-Parra, and E. Vives, Statistical Similarity Between the Compression of a Porous Material and Earthquakes, Phys. Rev. Lett. **110**, 088702 (2013).

[31] G. F. Nataf, P. O. Castillo-Villa, P. Sellappan, W. M. Kriven, E. Vives, A. Planes, and E. K. H. Salje, Predicting failure: Acoustic emission of berlinite under compression, J. Phys.: Condens. Matter **26**, 275401 (2014).

[32] J. P. Sethna, K. Dahmen, S. Kartha, J. A. Krumhansl, B. W. Roberts, and J. D. Shore, Hysteresis and Hierarchies: Dynamics of Disorder-Driven First-Order Phase Transformations, Phys. Rev. Lett. **70**, 3347 (1993).

[33] E. Vives and A. Planes, Avalanches in a fluctuationless first-order phase transition in a random-bond Ising model, Phys. Rev. B **50**, 3839 (1994).

[34] R. Ahluwalia and G. Ananthakrishna, Power-Law Statistics for Avalanches in a Martensitic Transformation, Phys. Rev. Lett. **86**, 4076 (2001).

[35] E. Bonnot, L. Mañosa, A. Planes, D. Soto-Parra, E. Vives, B. Ludwig, C. Strothkaemper, T. Fukuda, and T. Kakeshita, Acoustic emission in the fcc-fct martensitic transition of $Fe_{68.8}Pd_{31.2}$, Phys. Rev. B **78**, 184103 (2008).